NASA

DIRECTIONALITY OF BREMSSTRAHLUNG FROM RELATIVISTIC ELECTRONS IN SOLAR FLARES

CHARLES D. DERMER

REUVEN RAMATY

LABORATORY FOR HIGH ENERGY ASTROPHYSICS

National Aeronautics And Space Administration

Goddard Space Flight Center

Greenbelt, Maryland 20771

85-008

DIRECTIONALITY OF BREMSSTRAHLUNG FROM RELATIVISTIC ELECTRONS IN SOLAR FLARES

Charles D. Dermer[1] and Reuven Ramaty

NASA/Goddard Space Flight Center
Laboratory for High Energy Astrophysics
Greenbelt, MD 20771

To be published in the February 15, 1986 issue of the
Astrophysical Journal

September 1985

[1]NAS/NRC Resident Research Associate

ABSTRACT

We have calculated detailed angular and energy spectra of bremsstrahlung from anisotropic electron distributions in solar flares. We have compared the results to observations of gamma-ray limb-brightening and to data on the variation of the gamma-ray spectrum with flare position on the sun.

I. INTRODUCTION

Gamma-ray emission from solar flares consists of both continuum and lines (e.g. Ramaty et al. 1983a, Chupp 1984). The continuum is mostly bremsstrahlung produced by relativistic electrons. The lines result from nuclear reactions of energetic ions which excite both ambient and energetic nuclei, and produce neutrons and positrons. Line emission is then produced by deexcitations, neutron capture and positron annihilation. In addition, pion production may also be a significant source of gamma rays. Neutral pions decay into gamma rays directly, while charged pions decay into secondary positrons and electrons which produce gamma rays by bremsstrahlung.

Observations of solar flares with the gamma-ray spectrometer on SMM (Rieger et al. 1983) have shown that in the gamma-ray band, particularly at energies greater than 10 MeV, flares are seen preferentially from sites close to the solar limb. A likely explaration of these observations, consistent with the nonthermal nature of the relativistic electrons, is that the electron distribution in the emitting region is anisotropic. For nonthermal isotropic electron distributions, calculations of bremsstrahlung production in both the gamma-ray and hard X-ray bands have been performed by Bai (1977). For anisotropic electron distributions, calculations of bremsstrahlung production in the hard X-ray band have been made by, e.g. Elwert and Haug (1971), Brown (1972), Petrosian (1973), Bai and Ramaty (1978) and Emslie and Brown (1980).

However, there are no detailed calculations of bremsstrahlung production by anisotropic electron distributions in the energy range from ~0.1 MeV to ~100 MeV, which is the most important range for solar flare gamma-ray observations.

Gamma-ray production in solar flares most likely occurs in thick-target interactions (e.g. Ramaty et al. 1983a). In this model, the energetic particles produce gamma rays while losing their energy to the ambient medium through binary collisions and plasma processes. These processes modify the energy spectrum and angular distribution of the particles. Treatments of nonrelativistic and mildly relativistic electron transport in the solar atmosphere have been carried out (Leach and Petrosian 1981, Bai 1982, Emslie 1983), but a detailed calculation of bremsstrahlung production based on relativistic electron transport is unavailable.

We have limited the present investigation to the accurate calculation of bremsstrahlung production from electrons with given angular and energy distributions. The properties of these distributions depend on the acceleration mechanism and the transport process, but we do not attempt an investigation of these problems in the present paper. However, the constraints on the electron distributions that we obtain from the comparison of the calculations with the data should provide important insights into both the acceleration and transport questions.

In Section II we present the geometry of the interaction, the assumed distributions and the cross sections for bremsstrahlung production by relativistic electrons interacting in a fully ionized hydrogen plasma. We show the numerical results in Section III and we compare them with observations in Section IV.

II. ANALYSIS

The geometry of the elementary photon production event is shown in Figure 1. We take the **B**-axis along the magnetic field which we assume to be perpendicular to the photosphere. Let α be the pitch angle of the radiating electron and γ its Lorentz factor. Bremsstrahlung is observed at angle ψ with respect to the electron's original direction of motion. Taking the **z**-axis along the direction of observation, the colatitudes and azimuths of the electron and magnetic field are (ψ, ϕ) and (θ, ϕ_0), respectively. The pitch angle of the electron can then be written as

$$\cos\alpha = \cos\psi \cos\theta + \sin\psi \sin\theta \cos(\phi - \phi_0). \tag{1}$$

Let $N(\gamma, \Omega_\alpha)\, d\gamma\, d\Omega_\alpha$ be the number density of electrons with Lorentz factors between γ and $\gamma + d\gamma$ directed into solid angle $d\Omega_\alpha$ around Ω_α. Given the existence of an acceleration mechanism that makes specific predictions of the energy and angular distributions of the relativistic electrons, the form of $N(\gamma, \Omega_\alpha)$ could be determined from a treatment of the transport of the electrons in the solar atmosphere. However, such acceleration mechanisms have not yet been developed for solar flares and, moreover, the transport problem is very complicated, particularly if the effects of the magnetic turbulence are significant. For this reason, we are making the simplest assumption, namely that N is separable in energy and angle. We assume, in addition, that the angular distribution is azimuthally symmetric. Therefore,

$$N(\gamma, \Omega_\alpha) = n(\gamma)\, M(\cos\alpha). \tag{2}$$

We adopt the following normalizations:

$$2\pi \int_{-1}^{1} d\cos\alpha \; M(\cos\alpha) = 1 \quad \text{and} \quad \int_{2}^{\infty} d\gamma \; n(\gamma) = n_0, \tag{3}$$

where n_0 represents the number density of energetic electrons with kinetic energy greater than $m_e c^2$. If $n(\gamma)$ is chosen to be a power law in kinetic energy,

$$n(\gamma) = n_0 \; (s-1) \; (\gamma-1)^{-s}, \tag{4}$$

where s is the spectral index of the electron energy distribution.

We use the Bethe-Heitler formula (Koch and Motz 1959, Eq. 2BN) for the electron-proton bremsstrahlung differential cross section and the formula derived by Haug (1975a, Eq. A1) for the electron-electron bremsstrahlung differential cross section. The bremsstrahlung emissivity is then given by

$$q_{p,e}\,(\varepsilon,\cos\theta)\;[\text{photons}/(\text{cm}^3\text{-sec-sr-MeV})] = n_t \int d\Omega_\alpha \int d\gamma \cdot \beta c \cdot N(\gamma,\Omega_\alpha) \left(\frac{d^2\sigma}{d\varepsilon\, d\Omega_\psi}\right)_{p,e}, \tag{5}$$

where n_t is the target density and the subscripts p and e denote electron-proton and electron-electron bremsstrahlung, respectively. The contributions of these two components must be calculated separately.

Using equations (1)-(4) in equation (5), and changing variables and the order of integration, we obtain

$$q_{p,e}\,(\varepsilon,\cos\theta) = n_t n_0 (s-1) c \int_{\cos\psi_{max}(\varepsilon)}^{1} d\cos\psi \int_0^{2\pi} d\phi \; M(\cos\alpha) \cdot \int_{\gamma_{min}(\varepsilon,\cos\psi)}^{\infty} d\gamma \cdot \beta \cdot (\gamma-1)^{-s} \left(\frac{d^2\sigma}{d\varepsilon\, d\Omega_\psi}\right)_{p,e}. \tag{6}$$

The limits shown arise from kinematic restrictions. For electron-proton bremsstrahlung, $\gamma_{min} = 1+k$, where $k = \varepsilon/m_e c^2$, and $\cos\psi_{max} = -1$. For electron-electron bremsstrahlung,

$$\gamma_{min}(\varepsilon, u=\cos\psi) = \frac{1-k^2-uk(4k+u^2k^2)^{1/2}}{[(k-1)^2 - u^2k^2]} \tag{7}$$

and

$$\cos\psi_{max} = \begin{cases} 1-1/k, & k \geq 0.5 \\ -1, & k < 0.5 \end{cases} \tag{8}$$

(Haug 1975b).

Specific forms of $M(\cos\alpha)$ permit the integration over ϕ in equation (6) to be performed analytically. For a monodirectional electron beam, i.e $M(\cos\alpha)$ equal to a δ- function, equation (6) reduces to a single integral. The two more complicated forms of $M(\cos\alpha)$ that we consider are

$$M_r(\cos\alpha) = \frac{r \exp(r\cos\alpha)}{2\pi\ [\exp(r)-\exp(-r]}\ , \tag{9}$$

and

$$M_p(\cos\alpha) = \frac{(p+1)!!}{4\pi p!!} \sin^p\alpha\ . \tag{10}$$

Equation (9) describes an angular distribution that has a maximum at zero pitch angle and equation (10) describes a distribution that peaks at 90°. The anisotropy of these distributions increases with increasing r and p. If the magnetic field is perpendicular to the photosphere, equation (9) corresponds to a downward beamed distribution, while equation (10) corresponds to a distribution peaked at directions parallel to the photosphere. A downward beamed distribution could arise from an acceleration mechanism which produces

electrons beamed along the magnetic field, although Coulomb collisions would tend to partially disperse the beam. A distribution peaked parallel to the photosphere could arise from mirroring in a magnetic field gradient.

We have performed the ϕ- integral in equation (6), using either equation (9) or equation (10) with p = 2, 4, 6, 8 and 10, and the results are given in the Appendix. The remaining single or double integrals of equation (6) were performed numerically.

III. RESULTS

Bremsstrahlung emissivities for a monodirectional electron beam ($\theta = \psi$), for a variety of observing angles and for s=2.5 and s=3.5, are shown in Figures 2 and 3. The solid and dashed curves correspond to the contributions of e-p and e-e bremsstrahlung, respectively. These two components become identical at small observing angles and at high photon energies. The contribution of e-e bremsstrahlung falls off at low photon energies, due to the lack of a dipole moment in the electron-electron system, and at large observing angles, due to the recoil of the target electron. For a given observing angle,there is no e-e bremsstrahlung above a maximum photon energy which is given by equation (8).

The bremsstrahlung spectrum from a monodirectional electron beam depends on the observing angle θ. As can be seen in Figures 2 and 3, the photon spectrum is flatter for smaller observing angles, and for a given observing angle it steepens above a characteristic energy on the order of $m_e c^2/\theta$, for small θ. For large observing angles, the photon spectrum is quite steep, but its shape does not depend much on angle. The angular distribution of the bremsstrahlung from such a beam is much more anisotropic at high photon energies than at low energies. We note that at high photon energies (e.g. >10

MeV) the emissivity falls off very rapidly with observing angle at small angles, but then flattens out at large angles.

Bremsstrahlung emissivities obtained by summing the e-p and e-e contributions for the distributions (9) and (10) with s = 2.5 are shown in Figures 4, 5, and 6 for three observing angles and a variety of anisotropy parameters r and p. Similar results are shown in Figures 7, 8, and 9 for s = 3.5. The isotropic emissivities shown in these figures are in good agreement with the results obtained previously by Bai (1977).

All bremsstrahlung spectra shown in Figures 4-9, except those corresponding to the distribution (10) at 180°, exhibit a low-energy portion that is steeper than the parent electron spectrum and a high-energy portion that is flatter. This is due to the fact that at high energies a much larger fraction of the emission is from electrons moving at small angles to the observer than at low energies and, as we have seen, the photon spectrum from these electrons is flatter than that from electrons moving at large angles. The flattening of the photon spectrum does not occur at 180° for the distribution (10), because there are not enough particles moving at sufficiently small angles to the observer for the values of p that we consider.

The transition energy between the flatter high-energy portions of the spectra and steeper low-energy portions increases with increasing r and p and with increasing angle between the directions of observation and maximum anisotropy. In both cases the fraction of the electrons moving at small angles to the observer decreases and therefore only at increasingly high energies does the contribution of these electrons outweigh that of electrons moving at large angles.

We have integrated the differential emissivities over photon energy.

Integrated photon emissivities, for energies between 0.1 and 0.316 MeV, greater than 0.316 MeV, and greater than 10 MeV, are shown for a variety of r's and p's as functions of observation angle in Figures 10, 11, and 12 for s = 2.5, and in Figures 13, 14, and 15 for s = 3.5. The angular distribution of the radiation depends on both the assumed angular distribution of the electrons and the intrinsic angular dependence of the bremsstrahlung. The pattern of the radiation is dominated by the electron distribution at high photon energies, but only if the electron anisotropies are not too large. At higher anisotropies, the radiation pattern is determined predominantly by the angular distribution of the bremsstrahlung and is essentially independent of the angular distribution of the electrons.

To illustrate these effects for the distribution (9) and $-1<\cos\theta<0$ (i.e. a downward-peaked electron distribution observed in the backward hemisphere), we have approximated the emissivities shown in Figures 10 to 15 by the function $\exp(r'\cos\theta)$, and determined r', the anisotropy parameter of the radiation, by fitting this function to the calculations. The results are given in Table 1.

As can be seen, at photon energies >10 MeV, r'= r up to large values of r ($\lesssim$ 5), while at lower photon energies, r' is close to r only for low r($\lesssim$2 for >0.316 MeV). Also, for a given photon energy range, as r becomes large enough, r' becomes independent of r and takes on values that only reflect the angular distribution of the bremsstrahlung. We note that in the angular range under consideration ($90^0<\theta<180^0$), and at photon energies > 10 MeV, the radiation pattern is most anisotropic at r≈7 and declines as r is increased further This is a consequence of the flattening of the relativistic electron bremsstrahlung at large angles, as was noted earlier.

IV. COMPARISON WITH OBSERVATIONS

Observations of solar flares with the gamma-ray spectrometer on SMM revealed (Rieger et al. 1983) a center-to-limb variation which strongly suggests that the gamma-ray emission is anisotropic. This center-to-limb variation has been studied at photon energies > 0.3 MeV and > 10 MeV (E.L. Chupp and D.J. Forrest, private communication, 1985). In both of these energy ranges, the flares are observed preferentially near the solar limb. At photon energies greater than 10 MeV, more than 85% of the flares were observed at longitudes between $64° \lesssim \ell \lesssim 90°$, or $0.9 \lesssim \sin\ell \lesssim 1$, and at photon energies greater than 0.3 MeV, 42±5% of the flares were seen in the same longitude range. On the other hand, only 29% of the flares should have been observed at such longitudes if the emission were isotropic and optically thin.

Another observation which suggests that the gamma-ray emission from flares is anisotropic is the possible flattening of the spectral index with increasing longitude. From the data compiled by Chupp(1982), in the photon energy range 0.3-1.0 MeV, the index flattens by $\Delta s' \sim 1$ as ℓ varies from ~0° to ~90°.

To relate the limb-brightening results to our calculations, we must first assume a flare-size distribution. We take this distribution to be of the same form as that inferred from hard X-ray observations (Datlowe, Elcan and Hudson 1974; Lin et al. 1984). These observations suggest a distribution of the form A^{-1}, where A is the observed X-ray flux. The number of flares with gamma-ray emission measure exceeding EM should then be inversely proportional to EM, where $EM = V \cdot n_t \cdot n_0$ and V is the volume of the emitting region. To simplify the calculation, we assume that the flares occur at the solar equator, so that $\ell = 180° - \theta$.

The fraction of flares expected in the range of longitudes between 64° and 90° is then given by

$$R = \int_{64^0}^{90^0} d\ell\ Q_T \Big/ \int_{0^0}^{90^0} d\ell\ Q_T \ . \qquad (11)$$

Here Q_T is the total gamma-ray emission, which we take as the sum of a bremsstrahlung component as calculated above, and a nuclear component resulting from deexcitations, positron annihilation and neutron capture. This latter component is essentially isotropic, independent of the angular distribution of the parent protons and nuclei (e.g. Ramaty, Kozlovsky and Lingenfelter 1979). The bulk of the nuclear line emission appears at photon energies between about 0.4 and 8 MeV. Above 10 MeV and below 0.3 MeV the contribution of the nuclear lines is negligible. The total gamma-ray emission from flares should also contain emission from pions, but the analysis of one flare (June 21, 1980) indicates that at photon energies >10 MeV the contribution of the pion component is small (Ramaty et al. 1983b). While this may not apply to all flares, we assume that the pion component is negligible for the data that we consider here. Thus $Q_T = Q(-\cos\ell) + Q_n$, where Q_n is independent of ℓ.

We first compare the data to the calculations for the downward-peaked electron distribution. We have evaluated equation (11) with $Q(-\cos\ell) = \exp(-r'\cos\ell)$ and various values of K, where $K = Q_n/Q(\cos\ell = 0)$ is the ratio of the nuclear component to the bremsstrahlung component at the limb. The results are shown in Figure 16. Studies (Ramaty et al. 1983a,b; R. J. Murphy, private communication 1985) indicate that for photon energies greater than 0.3 MeV, K is about 0.1 to 0.3. Note that R tends to the isotropic value of 0.29 as $r' \to 0$.

Using the curve corresponding to K=0, the observed lower limit R>.85 for the >10 MeV emission implies that r'>5, which in turn implies (see Table 1) that 5<r<10. Thus, the observed limb brightening at > 10 MeV, if interpreted

in terms of a downward-beamed electron distribution, requires a strong anisotropy ($r>5$). But this anisotropy cannot be arbitrarily large ($r<10$) because for such a highly collimated downward beam, as we have discussed above, the angular distribution in the backward hemisphere in not sufficiently anisotropic to account for the observations.

The range $5<r<10$, deduced from the >10 MeV observations, implies for the >0.3MeV emission that $2.3<r'<2.9$ (see Table 1). Considering the data at >0.3 MeV, $R = 0.42 \pm .05$, we see from Figure 16 that this range of r' requires $K > 0.3$. By adding the effects of Compton backscatter, which would tend to isotropize the ~0.3 MeV emission (Bai 1977), we find that this limit could be lowered to ~0.2. Thus, if $K \approx 0.3$, both the high and low-energy observations can be understood in terms of a single value of r.

Considering the observed flattening of the spectral index from disk-center to limb, we deduce from Figures 4 and 6 and Figures 7 and 9 that in the photon energy range 0.3-1.0 MeV, $\Delta s'$ increases with increasing r up to a maximum value of ~1 at $r \approx 5$, and then decreases as r increases further. This maximum value is consistent with the observed increase $\Delta s' \approx 1$. In addition, as we have just seen, a single r in the range from 5 to 10 is consistent with the limb brightening at both >0.3 MeV and >10 MeV. Thus, an energy-independent anisotropy $r \approx 5$ would be consistent with all of the data. But the data would also allow the anisotropy to increase with energy, from $r \approx 5$ at >0.3 MeV to $r \approx 10$ at >10 MeV.

We next examine the distribution (10). By evaluating equation (11) with $Q(\cos\theta)$ given in Figures 12 and 15, we find that distributions with $p > 4$ will explain the observed > 10 MeV limb brightening. Then, by again evaluating equation (11) with the results of Figures 11 and 14 and various values of K, we find that to explain the > 0.3 MeV data K should be greater than about

0.4 for s=3.5 and K>0.5 for s=2.5. While these values of K could be reduced by the inclusion of the effects of the Compton backscatter, it appears that a single value of p is not adequate to explain the limb brightening observed at both high and low energies. But in this case also, the anisotropy could be energy dependent.

Regarding the flattening of the spectral index, larger values of $\Delta s'$ can be obtained from distribution (10) than from the downward-beamed distribution (9). From results similar to those shown in Figures 4 and 6 and Figures 7 and 9, we find $\Delta s' \approx 1$ for p=2 and $\Delta s' \approx 1.6$ for p=9.

Future observations, as well as further analysis of existing data, could provide additional insights into the question of the energy dependence of the electron anisotropy. In particular, if the electron anisotropy at >0.3 MeV were as large as determined at >10 MeV, the ratio of nuclear lines to bremsstrahlung for disk flares should on the average be larger than that for limb flares. Another test would be the observation of limb brightening in the 0.1-0.3 MeV range (see Figures 10 and 13 and Table 1), where the contribution of nuclear lines is negligible. However, the Compton backscatter must be taken into account in detail in any future analysis of data in this energy range.

The electron anisotropy has important consequences on the number of accelerated electrons implied by gamma-ray observations and hence also on the energy content in these electrons. For an isotropic electron pitch-angle distribution in the thick-target model, the number of electrons > 10 MeV for the June 21, 1980 flare was found to be $\sim 10^{31}$ (Ramaty et al. 1983b). This value will change depending on the assumed form of the electron anisotropy, but the determination of the magnitude of the change will require a detailed thick-target calculation with anisotropic injection of relativistic electrons. However, on the basis of the present calculations, we estimate

that for the downward-beamed distribution (Figs. 12 and 15) the value given above will be larger by a factor of ~15 for r=5 and ~850 for r=10. It has been pointed out (Vlahos et al. 1985) that the 30 MeV electron-to-proton ratio at the sun, deduced from gamma-ray and neutron observations assuming isotropic particle distributions, is lower than that observed in interplanetary space by about a factor of 100. This apparent discrepancy may be resolved by the downward-beamed distribution, since a larger number of electrons is needed to produce the same gamma-ray emission as for the isotropic case, while the number of protons deduced from the nuclear line emission is essentially independent of the anisotropy.

V. SUMMARY

We have calculated accurate bremsstrahlung energy spectra and angular distributions for a variety of electron distributions ranging from those peaked downwards into the photosphere to those aligned along the photosphere. General features can be summarized as follows:

(1) The photon spectra are steeper than the parent electron energy spectra at low energies and become flatter at high energies. The energy at which the flattening occurs depends on the electron anisotropy and on the observing angle. In the flatter portion, the radiation is mainly from electons moving within a cone of angle ~1/k to the oberving direction (k=photon energy/$m_e c^2$), while in the steeper portion the emission is mainly from electrons outside this cone.

(2) The photon angular distributions are similar to the electron angular distributions provided that the photon energies are high enough and the electron anisotropy is not too large. For large electron anisotropies and low

photon energies, the emission pattern follows the intrinsic bremsstrahlung radiation pattern. As a consequence, the degree of anisotropy of the photon angular distribution cannot be arbitrarily large. For example, for the downward-beamed electron distribution there is a maximum anisotropy for observing angles in the upward hemisphere.

(3) At a fixed photon energy, the spectral index increases or remains constant and the intensity of the bremsstrahlung emission decreases as the angle between the direction of observation and the direction of maximum particle number increases.

Referring to the observations of limb brightening and the flattening of the photon spectral index from disk-center to limb we conclude :

(4) For the downward-beamed distribution, the >10 MeV limb brightening implies that $5 < r < 10$. The > 0.3 MeV limb brightening is consistent with this range of r only if an isotropic nuclear gamma-ray component is taken into account. The observed flattening of the spectrum in the 0.3-1 MeV range suggests $r \simeq 5$. Thus, a single value of $r \simeq 5$ is consistent with all of the data. But an anisotropy which increases with energy (from $r \simeq 5$ at low energies to $r \simeq 10$) at high energies) would also be consistent with the observations.

(5) For the distribution peaking at directions parallel to the photosphere (equation 10), a value of $p > 9$ is required to explain the >10 MeV limb brightening. The change in spectral index can be accounted for by any value $p > 1$. However, even when a maximum nuclear line contribution is taken into account, the > 0.3 MeV limb-brightening requires that p decrease to a value

< 3 at ~0.3 MeV.

(6) The number of relativistic electrons at the sun implied by the downward-beamed distribution is larger by a factor of ~10 to ~10^3 than that deduced previously assuming an isotropic electron distribution. If a downward-beamed distribution is assumed, then, for at least one flare, the relativistic electron-to-proton ratio at the sun is similar to that observed in interplanetary space.

(7) Our calculations have not allowed for the possibility of the variation with energy of the electron angular distribution. Future calculations, incorporating the effects of electron transport, should take this possibility into account. Future simultaneous observations of the frequency of flare occurence, of the variation of the spectral index and of the ratio of bremsstrahlung to nuclear line emission could then provide much more detailed information on the acceleration, interaction and transport of relativistic electrons.

Acknowledgement We wish to thank Dr. E. Haug for useful comments on the manuscript.

APPENDIX

The value of the ϕ-integral for the function defined in equation (9) is given by

$$\int_0^{2\pi} d\phi \; M_r(\cos\alpha) = \frac{r \exp(r\cos\psi\cos\theta)}{[\exp(r) - \exp(-r)]} \sum_{j=0}^{\infty} \frac{(r\sin\psi\sin\theta)^{2j}}{2^{2j}(j!)^2} . \tag{A1}$$

The value of the ϕ- integral for equation (10) is

$$I_p \equiv \frac{(p+1)!!}{4\pi p!!} \int_0^{2\pi} d\phi \; \sin^p\alpha . \tag{A2}$$

The results for p = 2,4,6,8 and 10 are

$$I_2 = \frac{3a}{4}\left(1 + \frac{d}{2}\right) , \tag{A3}$$

$$I_4 = \frac{15a^2}{16}\left[1 + \frac{1}{2}(b^2+2d) + \frac{3d^2}{8}\right], \tag{A4}$$

$$I_6 = \frac{35a^3}{32}\left[1 + \frac{3}{2}\left(1 + \frac{3d}{4}\right)(b^2+d) + \frac{15d^3}{48}\right], \tag{A5}$$

$$I_8 = \frac{315a^4}{256}\left[1+ \left(1+ \frac{5d^2}{8}\right)(3b^2+2d) + \frac{3}{8}(12b^2d+b^4+6d^2) + \frac{35d^4}{128}\right], \tag{A6}$$

$$I_{10} = \frac{693a^5}{512}\left[1 + \frac{5}{2}\left(1 + \frac{35d^3}{64}\right)(2b^2+d) + \frac{5}{8}\left(3 + \frac{5d}{2}\right)(b^4+ 6b^2d + 2d^2) + \frac{63d^5}{256}\right], \tag{A7}$$

where $a = (1-\cos^2\psi\cos^2\theta)$, $b = -2(\cos\psi\cos\theta\sin\psi\sin\theta)/a$, and $d = -(\sin^2\psi\sin^2\theta)/a$.

REFERENCES

Bai, T. 1977, Ph. D. Thesis, University of Maryland.

-----. 1982, Ap. J., **259**, 341.

Bai, T., and Ramaty, R. 1978, Ap. J., **219**, 705.

Brown, J. C. 1972, Solar Phys., **26**, 441.

Chupp, E. L. 1982, in Gamma Ray Transients and Related Astrophysical Phenomena, ed. R. E. Lingenfelter, H. S. Hudson, and D. M. Worrall (New York: American Institute of Physics), p. 363.

Chupp, E. L. 1984, Ann. Rev. Astron. Astrophys., **22**, 359.

Datlowe, D. W., Elcan, M. J., and Hudson, H. S. 1974, Solar Phys., **39**, 155.

Elwert, G., and Haug, E. 1971, Solar Phys., **20**, 413.

Emslie, A. G. 1983, Ap. J., **271**, 367.

Emslie, A. G., and Brown, J. C. 1980, Ap. J., **237**, 1015.

Haug, E. 1975a, Zs. Naturforsch., **30a**, 1099.

Haug, E. 1975b, Solar Phys., 45, 433.

Koch, H. W., and Motz, J. W. 1959, Rev. Mod. Phys., **31**, 920.

Leach, J., and Petrosian, V. 1981, Ap. J., **251**, 781.

Lin, R. P., Schwartz, R. A., Kane, S. R., Pelling, R. M., and Hurley, K. C. 1984, Ap. J., **283**, 421.

Petrosian, V. 1973, Ap. J., 186, 291.

Ramaty, R., Kozlovsky, B., and Lingenfelter, R.E. 1979, Ap. J. (Suppl.), **40**, 487.

Ramaty, R., Murphy, R. J., Kozlovsky, B., and Lingenfelter, R. E. 1983a, Solar Phys., **86**, 395.

--------. 1983b, Ap. J., **273**, L41.

Rieger, E., Reppin, C., Kanbach, G., Forrest, D. J., Chupp, E. L., and Share, G. H. 1983, in 18th International Cosmic Ray Conference (Late Papers), Bangalore, **10**, 338.

Vlahos, L., et al. 1985, in Energetic Phenomena in Solar Flares, ed. M. R. Kundu and B. Woodgate, in press.

FIGURE CAPTIONS

Fig. 1. Geometry of the elementary scattering event.

Fig. 2. Emissivity of a monodirectional beam of electrons for a variety of observing angles. The solid lines refer to the contribution of electron-proton bremsstrahlung and the dashed lines refer to the contribution of electron-electron bremsstrahlung. The energy spectrum of the electron beam is a power law in kinetic energy with spectral index s=2.5.

Fig. 3. Same as for Fig. 2, but with s=3.5.

Fig. 4. Total bremsstrahlung emissivities from electrons with angular distributions (9) or (10), for a variety of values r and p, respectively. The energy spectrum of the electrons is a power law in kinetic energy with spectral index s = 2.5. The observing angle θ=90°.

Fig. 5. Same as for Fig. 4, but with θ=150°.

Fig. 6. Same as for Fig. 4, but with θ=180°.

Fig. 7. Same as for Fig. 4, but with s=3.5.

Fig. 8. Same as for Fig. 4, but with s=3.5 and θ=150°.

Fig. 9. Same as for Fig. 4, but with s=3.5 and θ=180°.

Fig. 10. Total bremsstrahlung emissivities integrated between photon energies 0.10 and 0.316 MeV from energetic electrons with angular distributions given by equations (9) or (10), for a variety of values r and p, respectively. The energy spectrum of the electrons is a power law in kinetic energy with spectral index s=2.5.

Fig. 11. Same as for Fig. 10, but integrated above 0.316 MeV.

Fig. 12. Same as for Fig. 10, but integrated above 10.0 MeV.

Fig. 13. Same as for Fig. 10, but with s=3.5.

Fig. 14. Same as for Fig. 10, but integrated above 0.316 MeV and with s=3.5.

Fig. 15. Same as for Fig. 10, but integrated above 10.0 MeV and with s=3.5.

Fig. 16. The ratio of flares that would be observed in the range of longitudes $64° < \ell < 90°$ ($0.9 < \sin\ell < 1$) to those that would be observed in the range $0° < \ell < 90°$ if the bremsstrahlung emissivity is proportional to $\exp(r'\cos\theta)$ and an isotropic component is included. The relative contribution of the isotropic component is characterized by the value of K, where K is the ratio of the isotropic component to the bremsstrahlung component at $\ell = 90°$.

Charles D. Dermer

Code 665

NASA/Goddard Space Flight Center

Greenbelt, MD 20771

Reuven Ramaty

Code 665

NASA/Goddard Space Flight Center

Greenbelt, MD 20771

TABLE 1

The dependence of r' on r for various photon energies and electron spectral indexes

	0.1-0.316MeV		>0.316MeV		>10MeV	
r	s=2.5	s=3.5	s=2.5	s=3.5	s=2.5	s=3.5
1	.79	.65	.92	.90	1.0	1.0
2	1.2	1.2	1.8	1.7	2.0	2.0
3	1.6	1.6	2.6	2.4	3.0	3.0
5	1.7	2.0	2.9	2.7	5.0	5.0
7	1.7	2.1	2.6	2.6	6.5	6.3
10	1.7	2.2	2.4	2.6	5.2	4.6
20	1.7	2.3	2.3	2.6	3.4	3.4

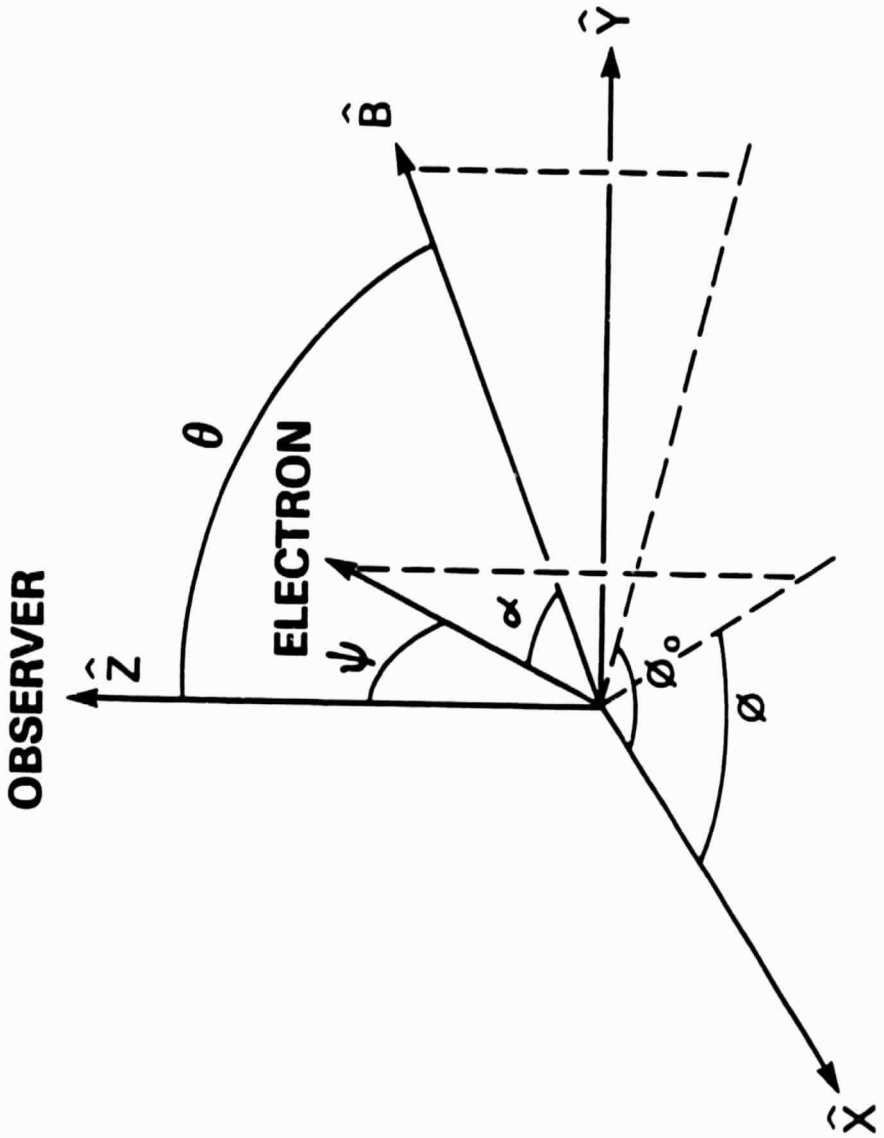

Fig. 1

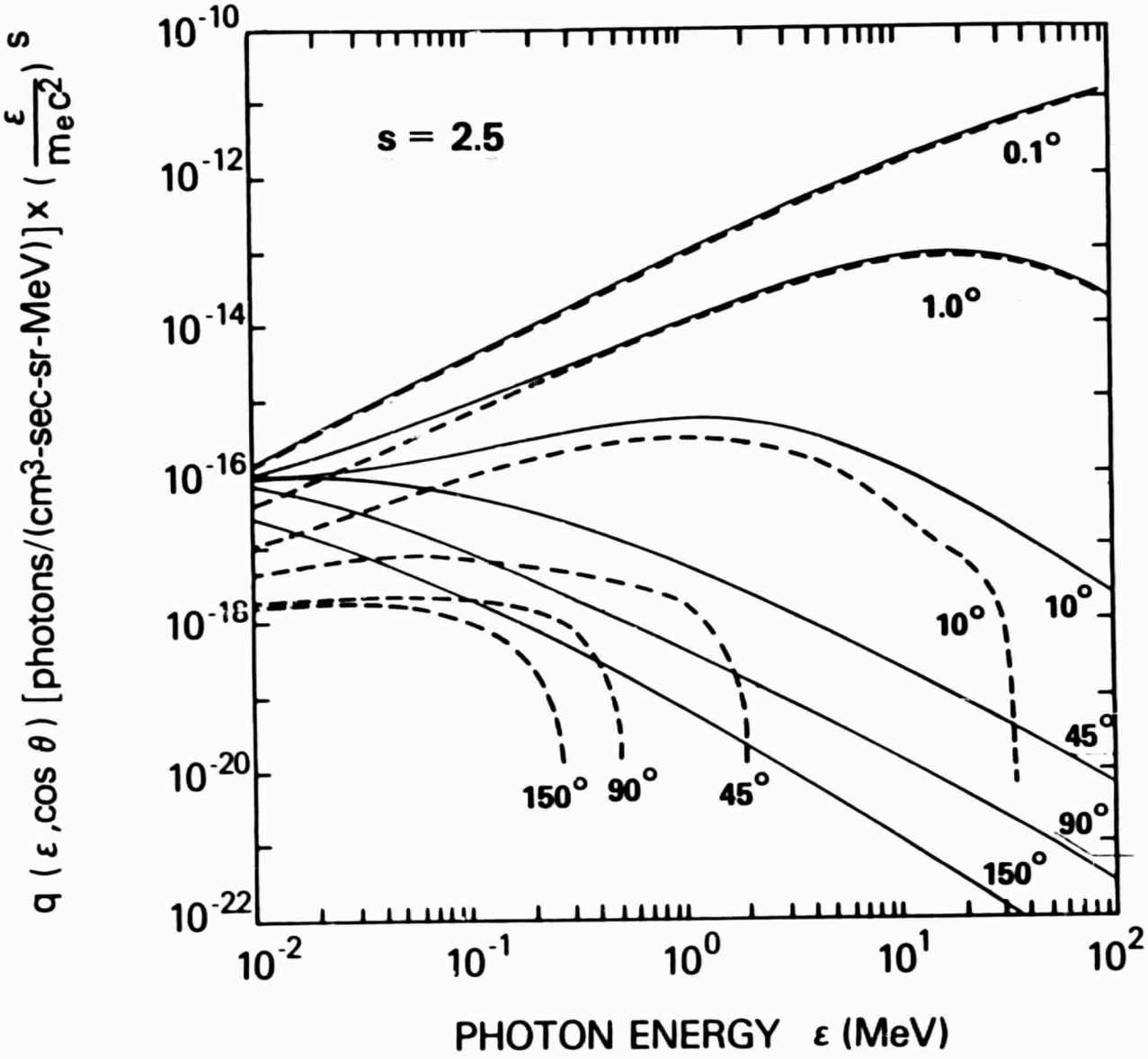
s = 2.5
0.1°
1.0°
10°
10°
45°
90°
150°
150°
90°
45°
10^{-10}
10^{-12}
10^{-14}
10^{-16}
10^{-18}
10^{-20}
10^{-22}
10^{-2}
10^{-1}
10^{0}
10^{1}
10^{2}
q (ε ,cos θ) [photons/(cm³-sec-sr-MeV)] x (ε / m_e c²) s
PHOTON ENERGY ε (MeV)

Fig. 2

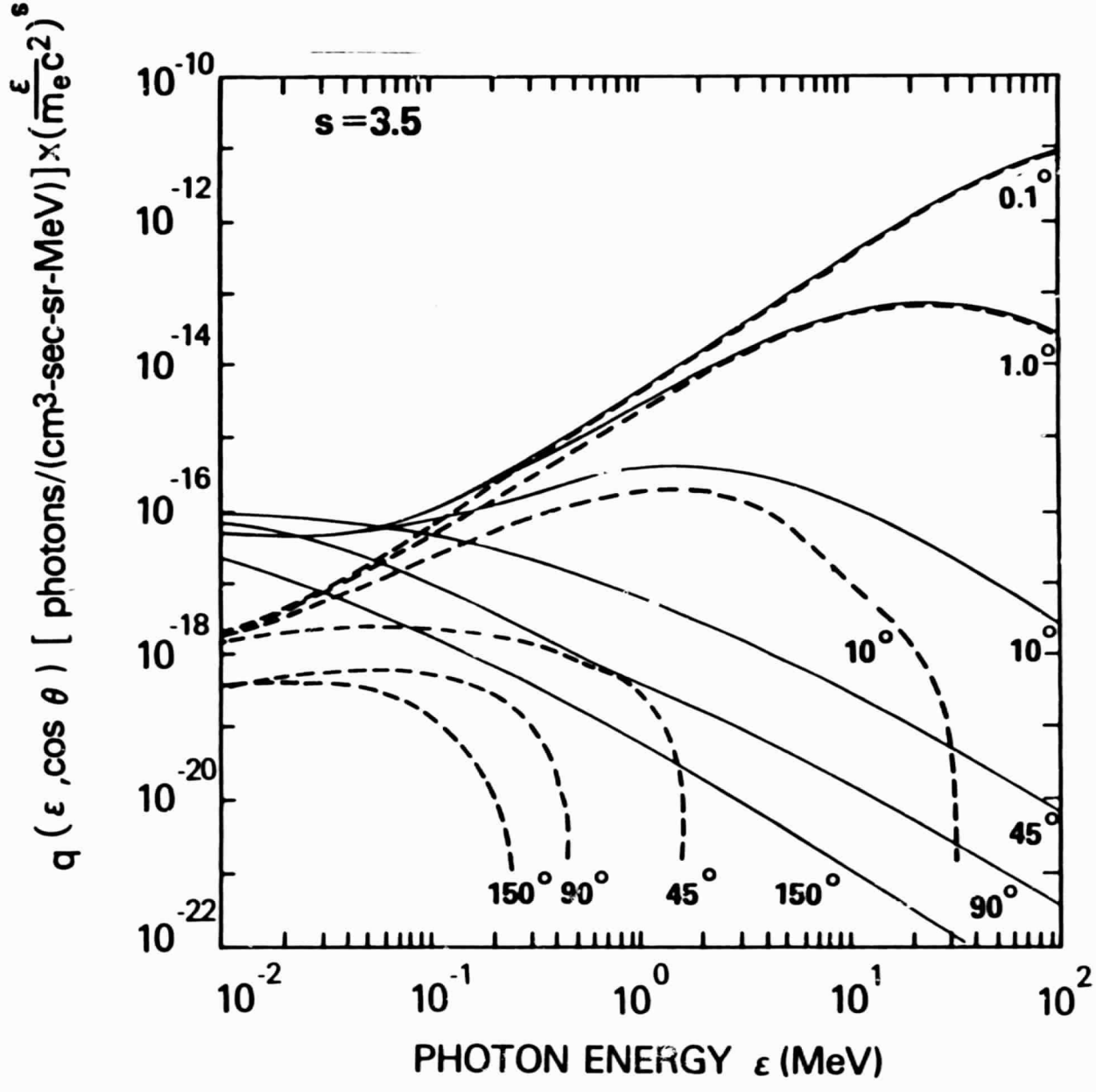
s =3.5
0.1°
1.0°
10°
10°
45°
90°
150°
150°
90°
45°
$q(\varepsilon, \cos\theta)$ [photons/(cm^3-sec-sr-MeV)] $\times(\frac{\varepsilon}{m_e c^2})^s$
PHOTON ENERGY ε (MeV)
10^{-10}
10^{-12}
10^{-14}
10^{-16}
10^{-18}
10^{-20}
10^{-22}
10^{-2}
10^{-1}
10^{0}
10^{1}
10^{2}

Fig. 3

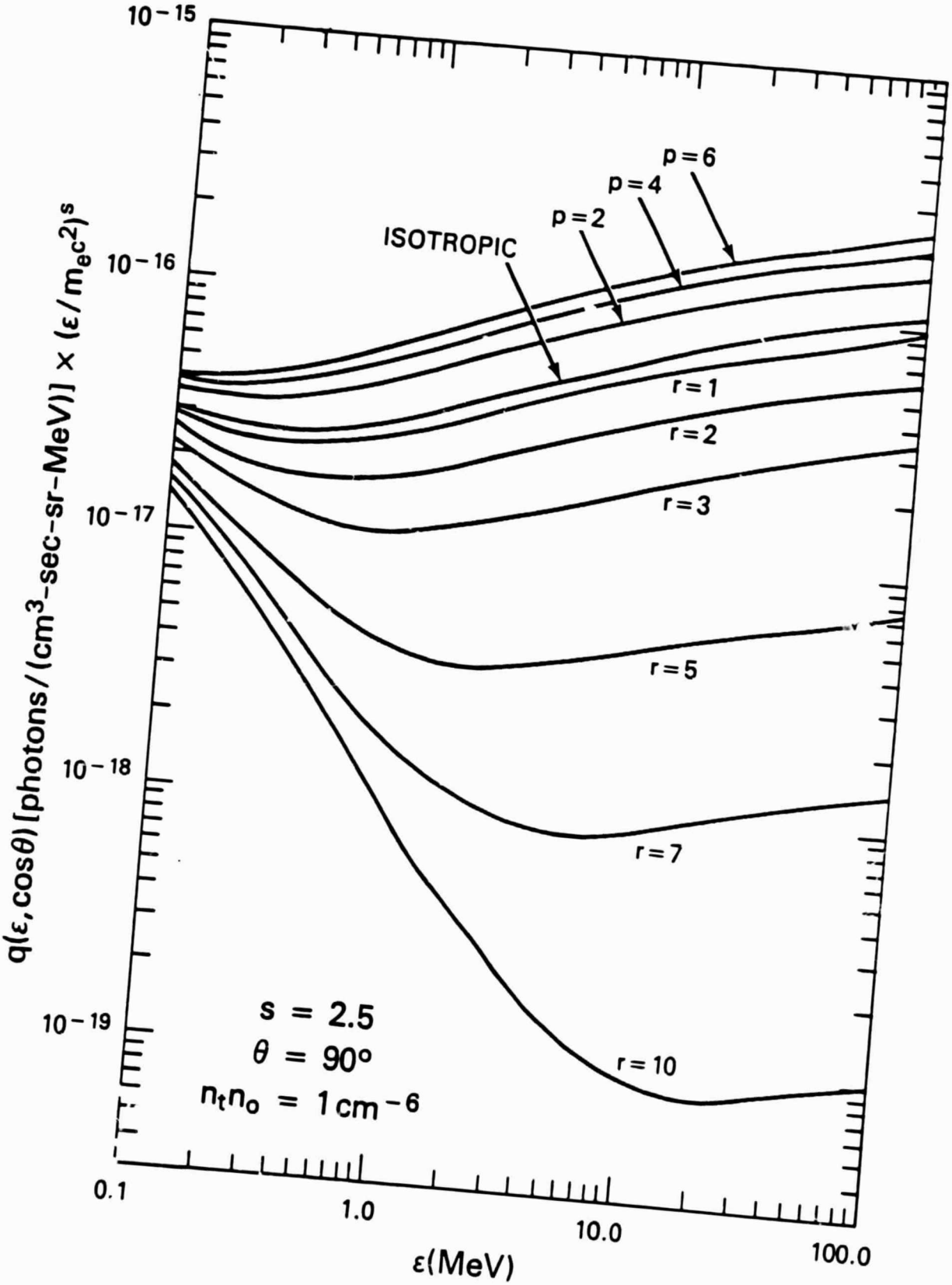
10^{-15}
10^{-16}
10^{-17}
10^{-18}
10^{-19}
$q(\varepsilon, \cos\theta)$ [photons/(cm^3-sec-sr-MeV)] × $(\varepsilon/m_ec^2)^s$
p = 6
p = 4
p = 2
ISOTROPIC
r = 1
r = 2
r = 3
r = 5
r = 7
r = 10
s = 2.5
θ = 90°
$n_t n_o$ = 1 cm^{-6}
0.1
1.0
10.0
100.0
ε(MeV)

Fig. 4

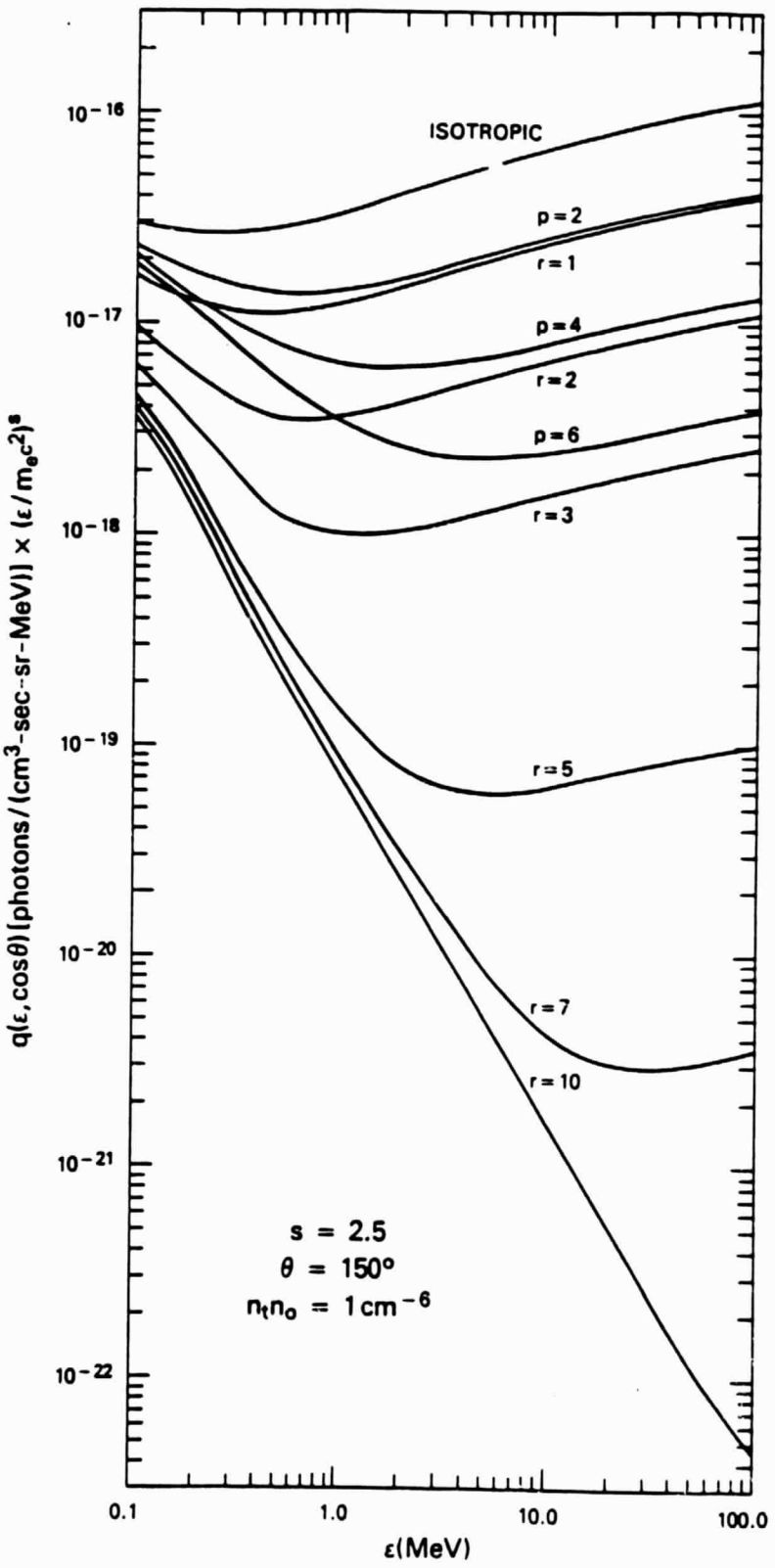
ISOTROPIC
p=2
r=1
p=4
r=2
p=6
r=3
r=5
r=7
r=10
s = 2.5
θ = 150°
$n_t n_o$ = 1 cm^{-6}
10^{-16}
10^{-17}
10^{-18}
10^{-19}
10^{-20}
10^{-21}
10^{-22}
0.1
1.0
10.0
100.0
ε(MeV)
q(ε, cosθ)[photons/(cm^3-sec-sr-MeV)] × (ε/$m_e c^2$)^s

Fig. 5

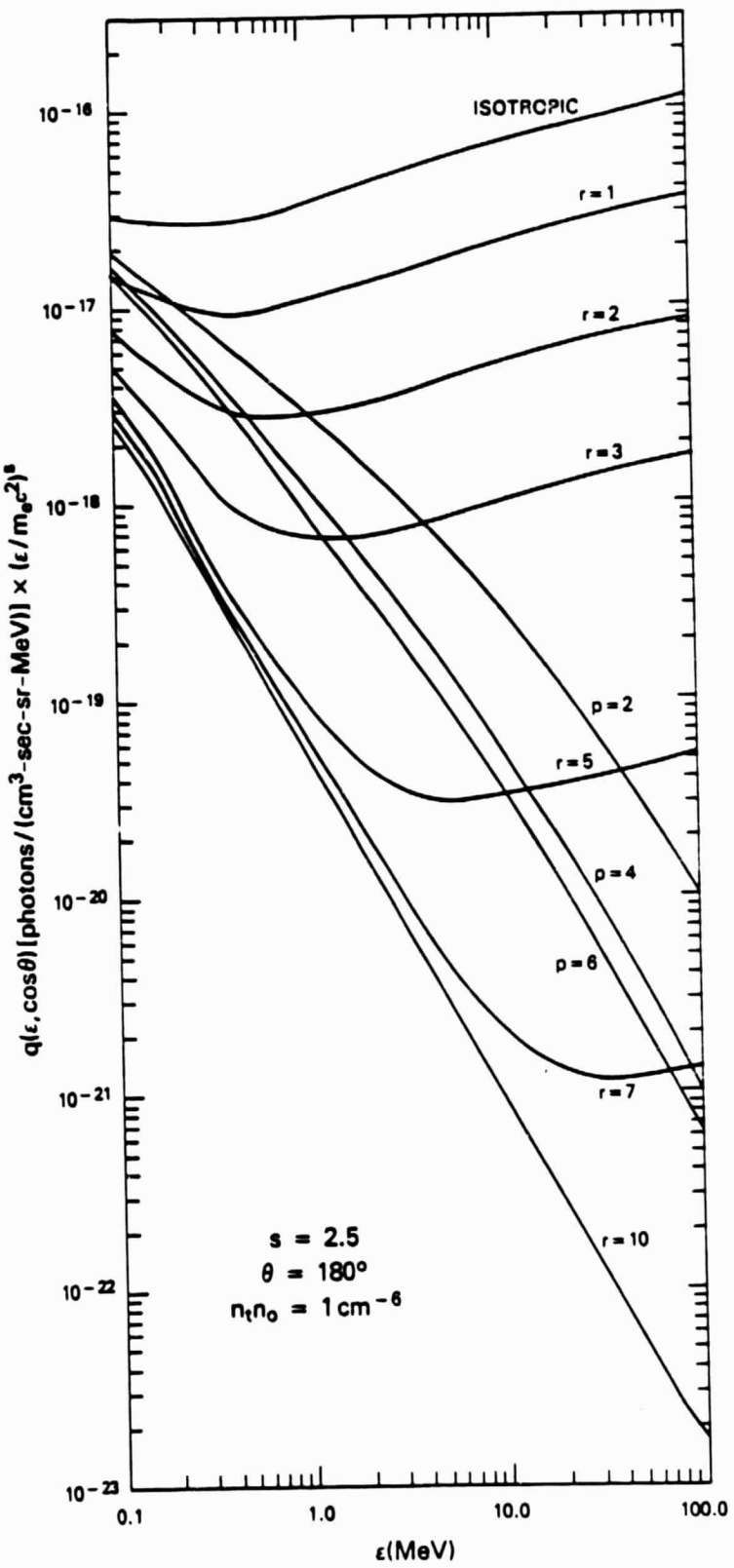
ISOTROPIC
r=1
r=2
r=3
p=2
r=5
p=4
p=6
r=7
r=10
s = 2.5
θ = 180°
$n_t n_o$ = 1 cm^{-6}
10^{-16}
10^{-17}
10^{-18}
10^{-19}
10^{-20}
10^{-21}
10^{-22}
10^{-23}
0.1
1.0
10.0
100.0
ε(MeV)
q(ε, cosθ)[photons/(cm^3-sec-sr-MeV)] × (ε/$m_e c^2$)^s

Fig. 6

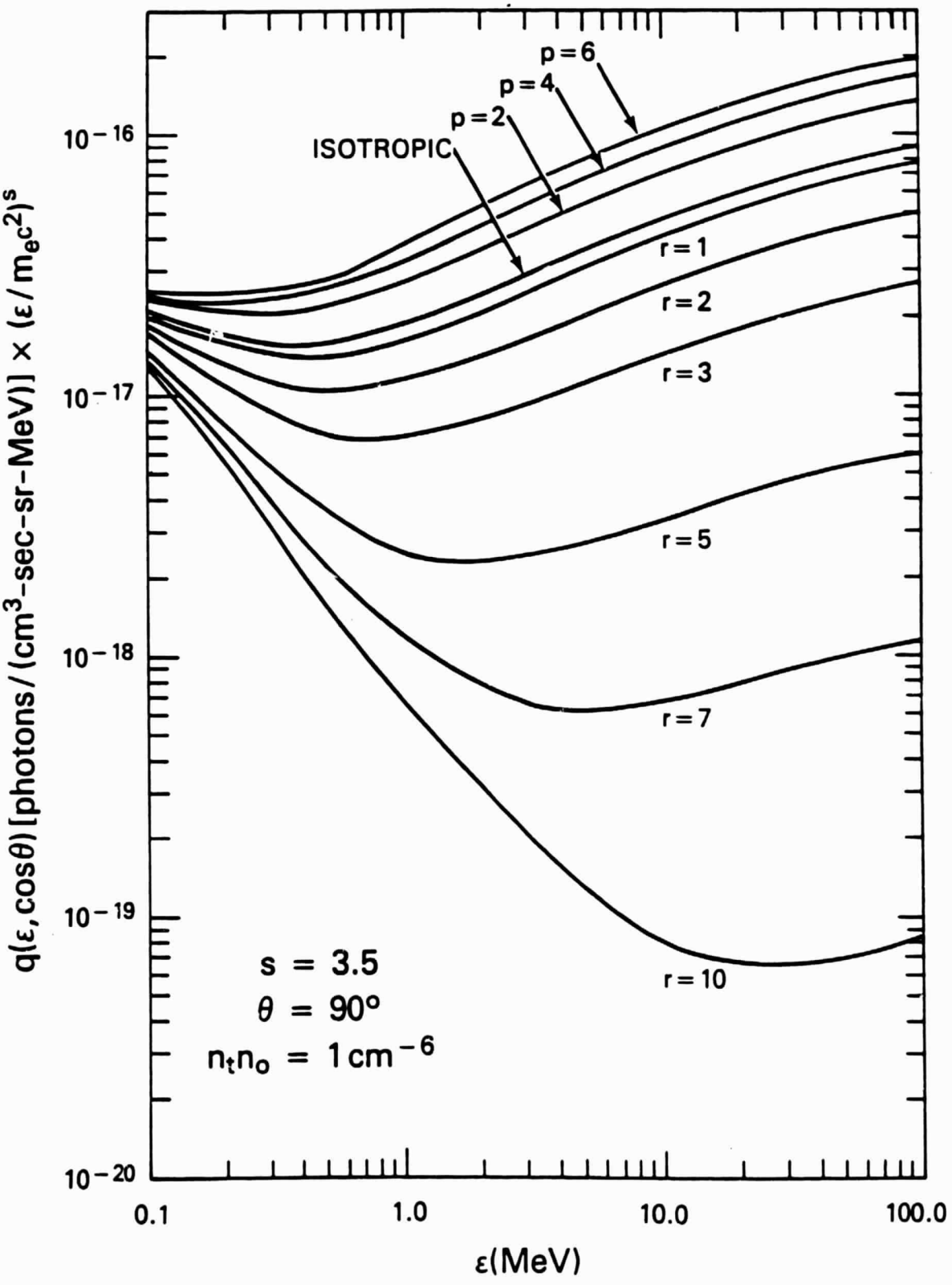
p = 6
p = 4
p = 2
ISOTROPIC
r = 1
r = 2
r = 3
r = 5
r = 7
r = 10
s = 3.5
θ = 90°
$n_t n_o = 1\,cm^{-6}$
10^{-16}
10^{-17}
10^{-18}
10^{-19}
10^{-20}
0.1
1.0
10.0
100.0
ε(MeV)
$q(\varepsilon, \cos\theta)$ [photons/$(cm^3$-sec-sr-MeV)] × $(\varepsilon / m_e c^2)^s$

Fig. 7

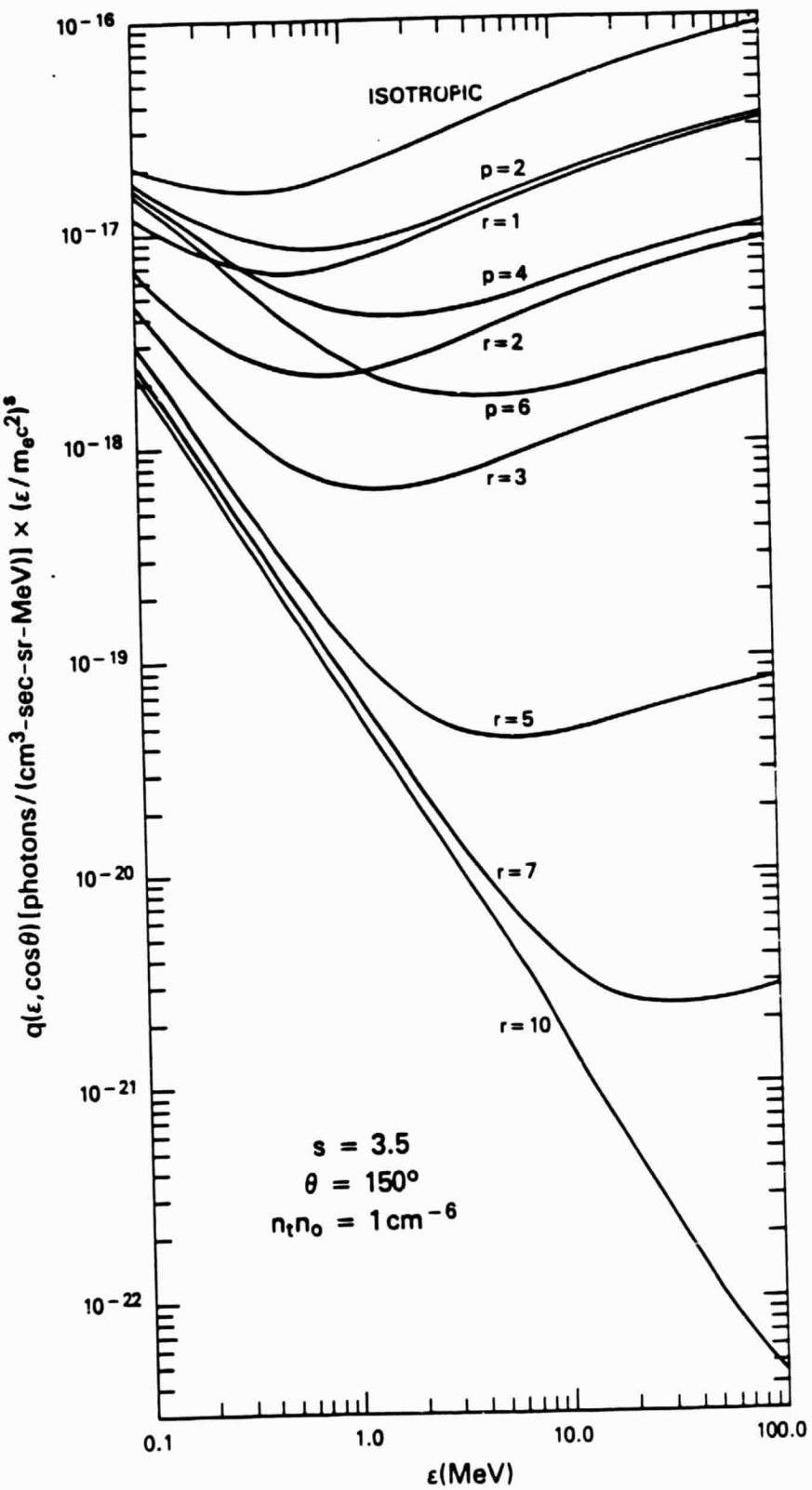
ISOTROPIC
p=2
r=1
p=4
r=2
p=6
r=3
r=5
r=7
r=10
s = 3.5
θ = 150°
$n_t n_o$ = 1 cm^{-6}
10^{-16}
10^{-17}
10^{-18}
10^{-19}
10^{-20}
10^{-21}
10^{-22}
0.1
1.0
10.0
100.0
ε(MeV)
$q(\varepsilon, \cos\theta)$[photons/(cm^3-sec-sr-MeV)] × $(\varepsilon/m_e c^2)^s$

Fig. 8

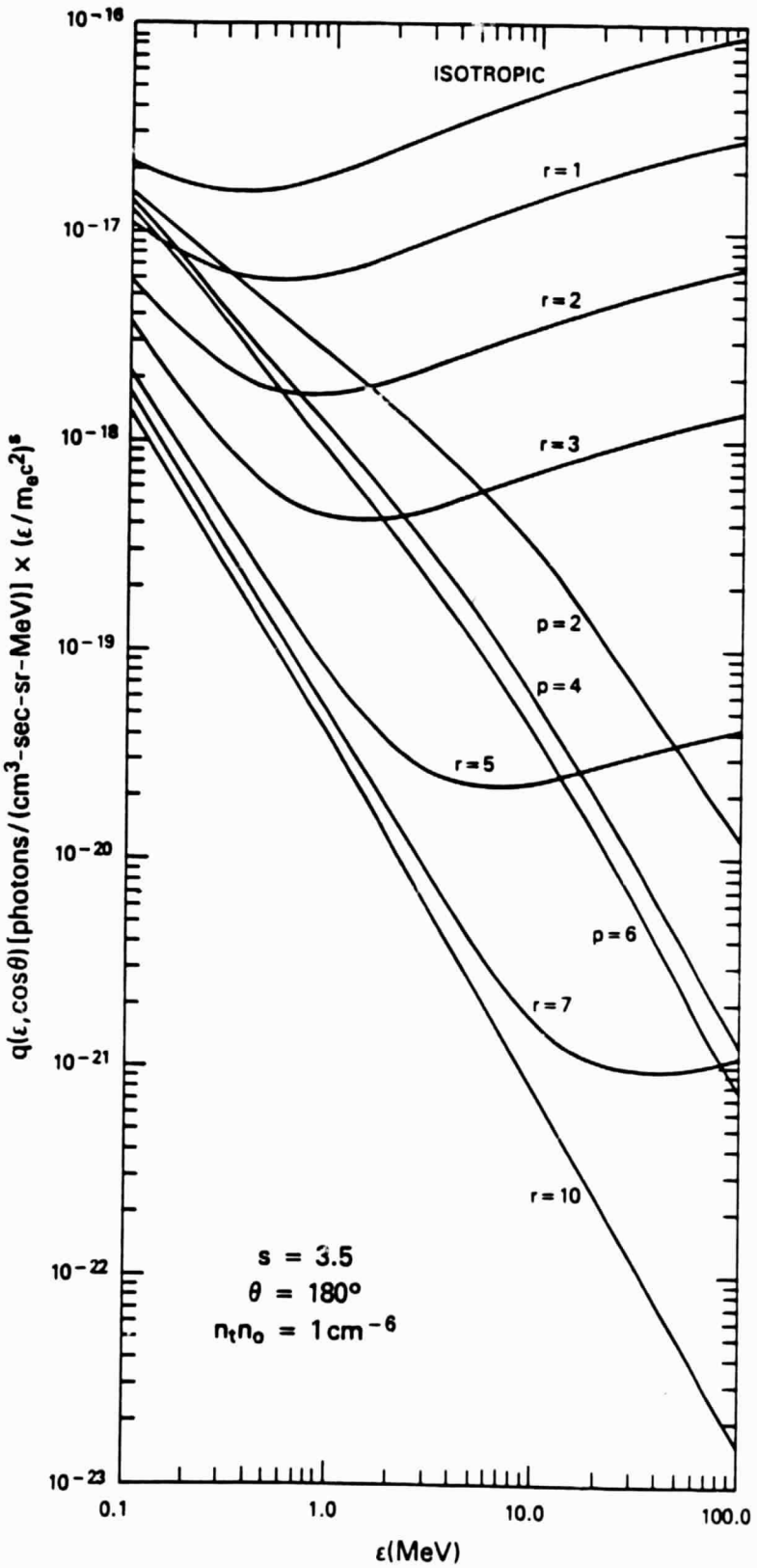
ISOTROPIC
r = 1
r = 2
r = 3
p = 2
p = 4
r = 5
p = 6
r = 7
r = 10
s = 3.5
θ = 180°
$n_t n_o$ = 1 cm^{-6}
10^{-16}
10^{-17}
10^{-18}
10^{-19}
10^{-20}
10^{-21}
10^{-22}
10^{-23}
0.1
1.0
10.0
100.0
ε(MeV)
q(ε, cosθ)[photons/(cm^3-sec-sr-MeV)] × (ε/$m_e c^2$)^s

Fig. 9

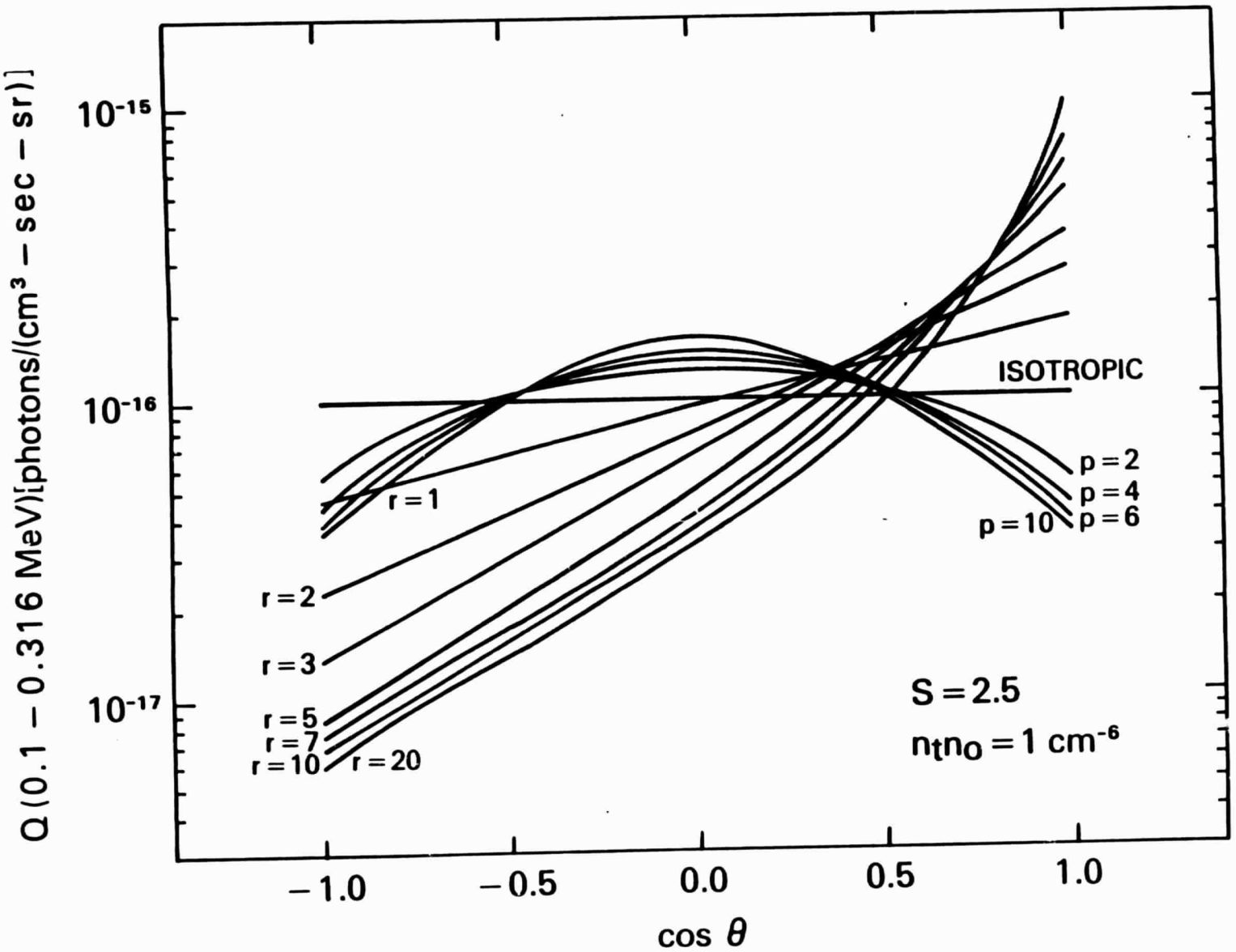
$Q(0.1 - 0.316\ MeV)[photons/(cm^3 - sec - sr)]$
10^{-15}
10^{-16}
10^{-17}
ISOTROPIC
p = 2
p = 4
p = 6
p = 10
r = 1
r = 2
r = 3
r = 5
r = 7
r = 10
r = 20
S = 2.5
$n_t n_o = 1\ cm^{-6}$
−1.0
−0.5
0.0
0.5
1.0
cos θ

Fig. 10

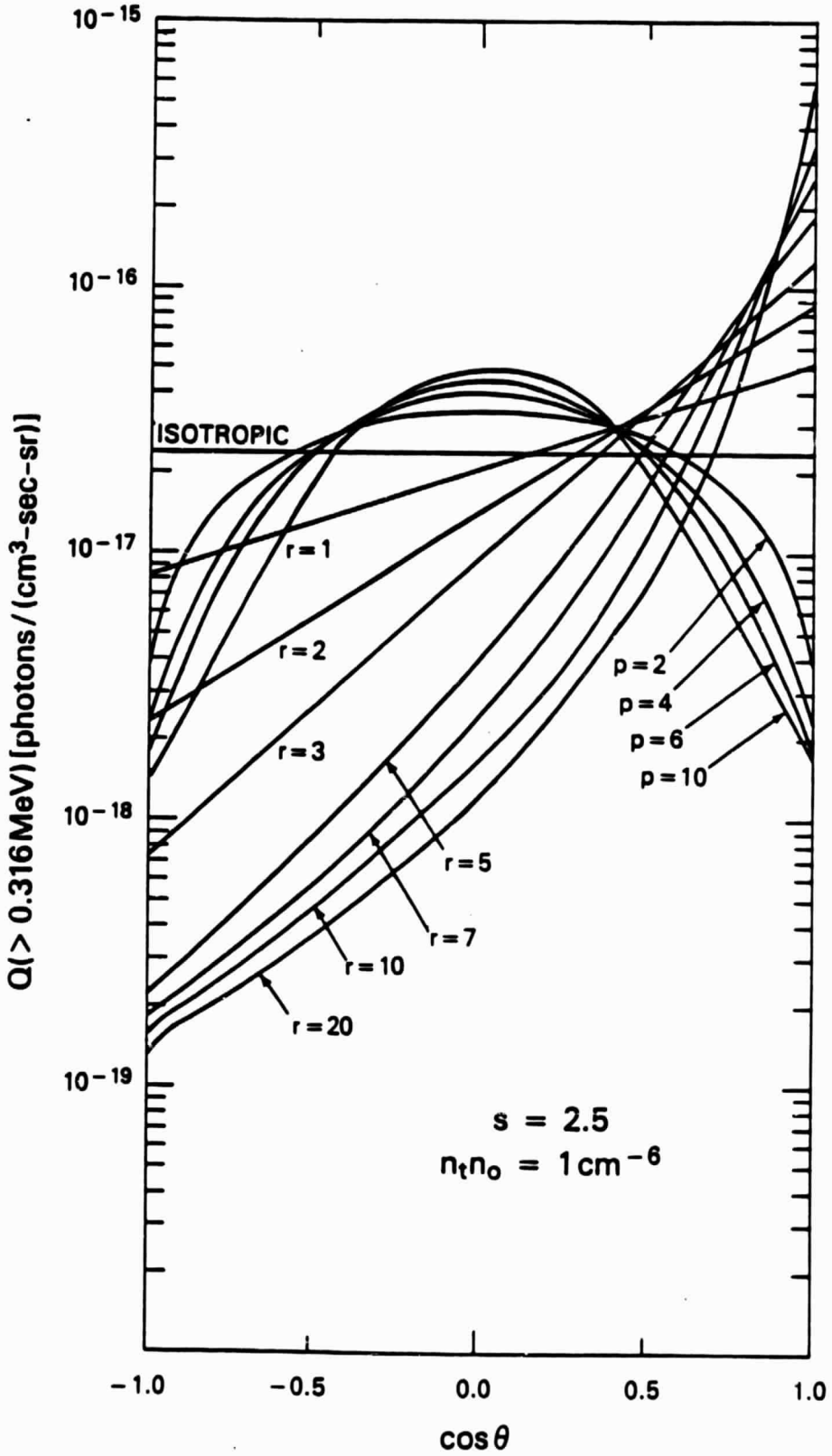
10^{-15}
10^{-16}
10^{-17}
10^{-18}
10^{-19}
$Q(> 0.316 MeV)$ [photons/(cm^3-sec-sr)]
ISOTROPIC
r = 1
r = 2
r = 3
r = 5
r = 7
r = 10
r = 20
p = 2
p = 4
p = 6
p = 10
s = 2.5
$n_t n_o = 1 cm^{-6}$
−1.0
−0.5
0.0
0.5
1.0
cos θ

Fig. 11

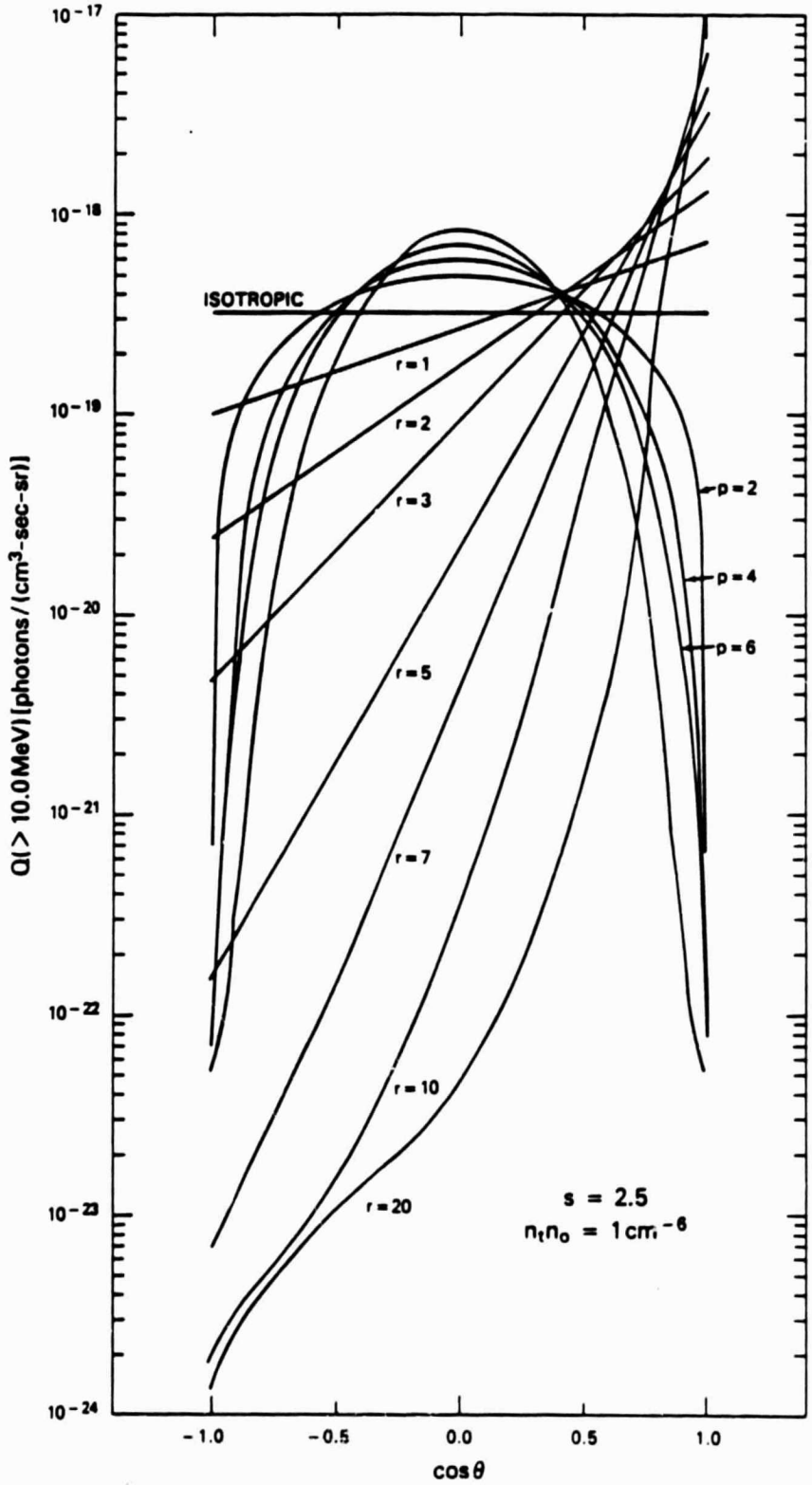
10^{-17}
10^{-18}
10^{-19}
10^{-20}
10^{-21}
10^{-22}
10^{-23}
10^{-24}
$Q(>10.0\,MeV)$ [photons/(cm^3-sec-sr)]
ISOTROPIC
r = 1
r = 2
r = 3
r = 5
r = 7
r = 10
r = 20
p = 2
p = 4
p = 6
s = 2.5
$n_t n_o = 1\,cm^{-6}$
-1.0
-0.5
0.0
0.5
1.0
cos θ

Fig. 12

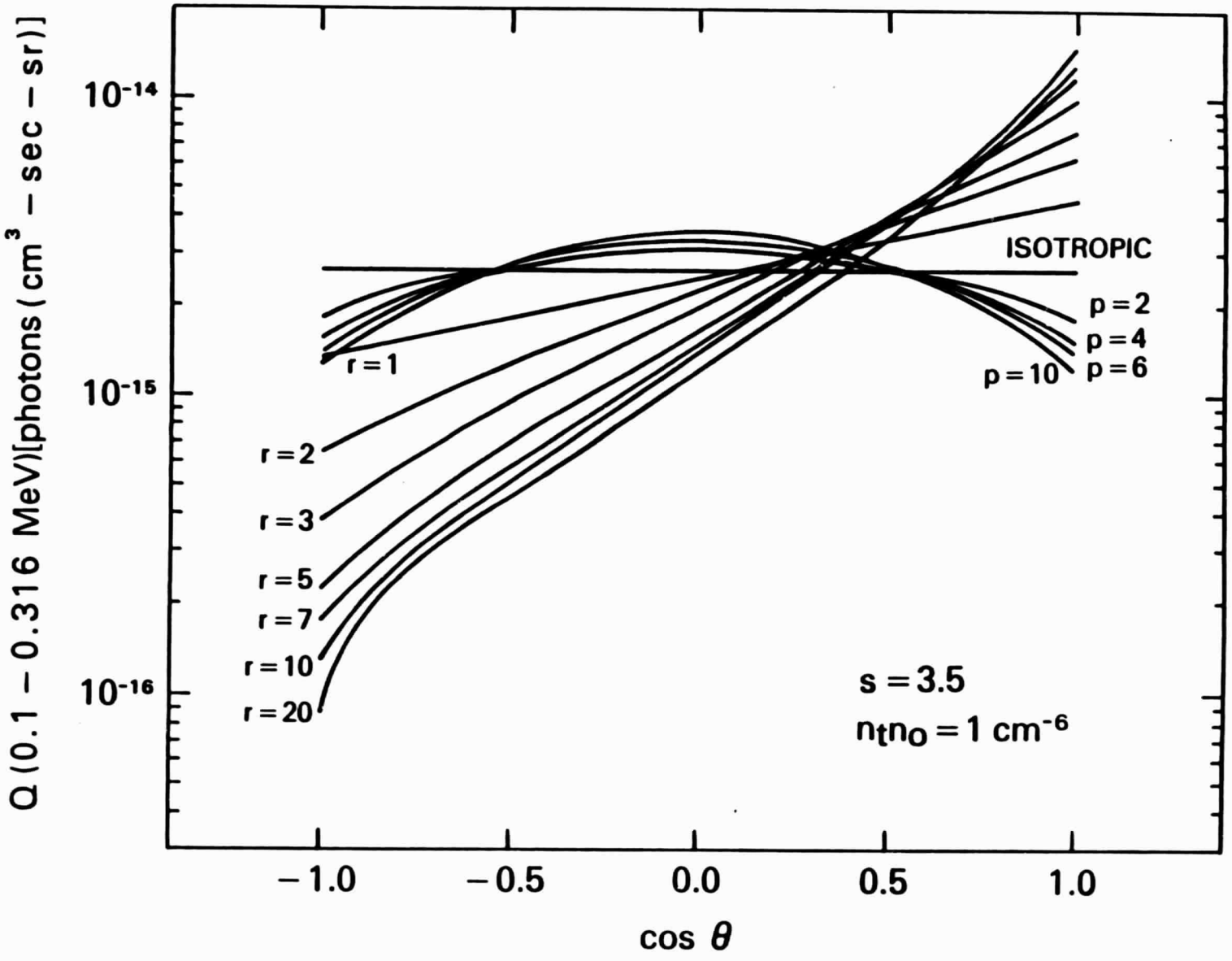
Q (0.1 – 0.316 MeV)[photons (cm³ – sec – sr)]
10⁻¹⁴
10⁻¹⁵
10⁻¹⁶
ISOTROPIC
p = 2
p = 4
p = 6
p = 10
r = 1
r = 2
r = 3
r = 5
r = 7
r = 10
r = 20
s = 3.5
n_t n_o = 1 cm⁻⁶
–1.0
–0.5
0.0
0.5
1.0
cos θ

Fig. 13

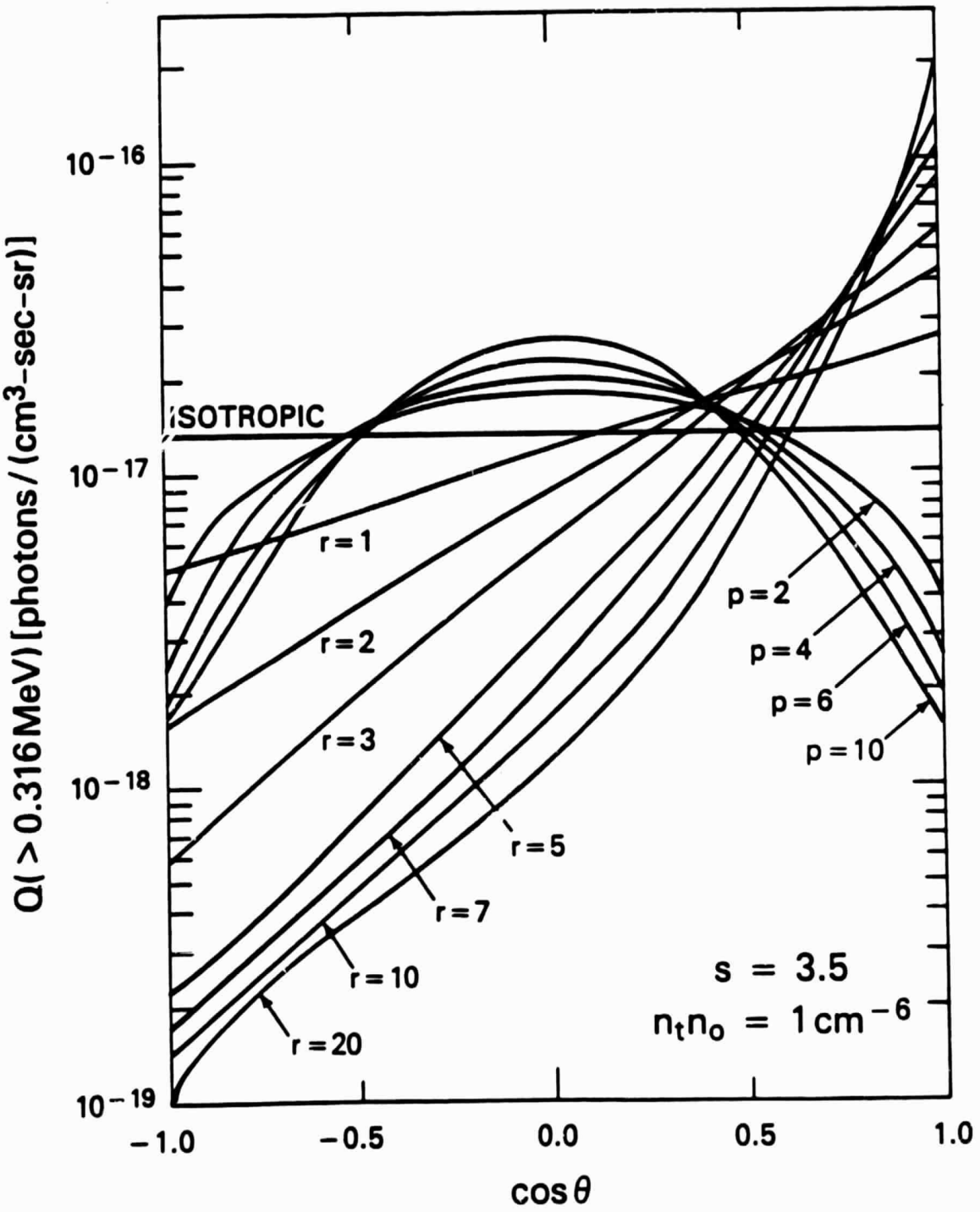
10^{-16}
10^{-17}
10^{-18}
10^{-19}
Q(>0.316MeV)[photons/(cm^3-sec-sr)]
ISOTROPIC
r=1
r=2
r=3
r=5
r=7
r=10
r=20
p=2
p=4
p=6
p=10
s = 3.5
$n_t n_o$ = 1cm^{-6}
−1.0
−0.5
0.0
0.5
1.0
cos θ

Fig. 14

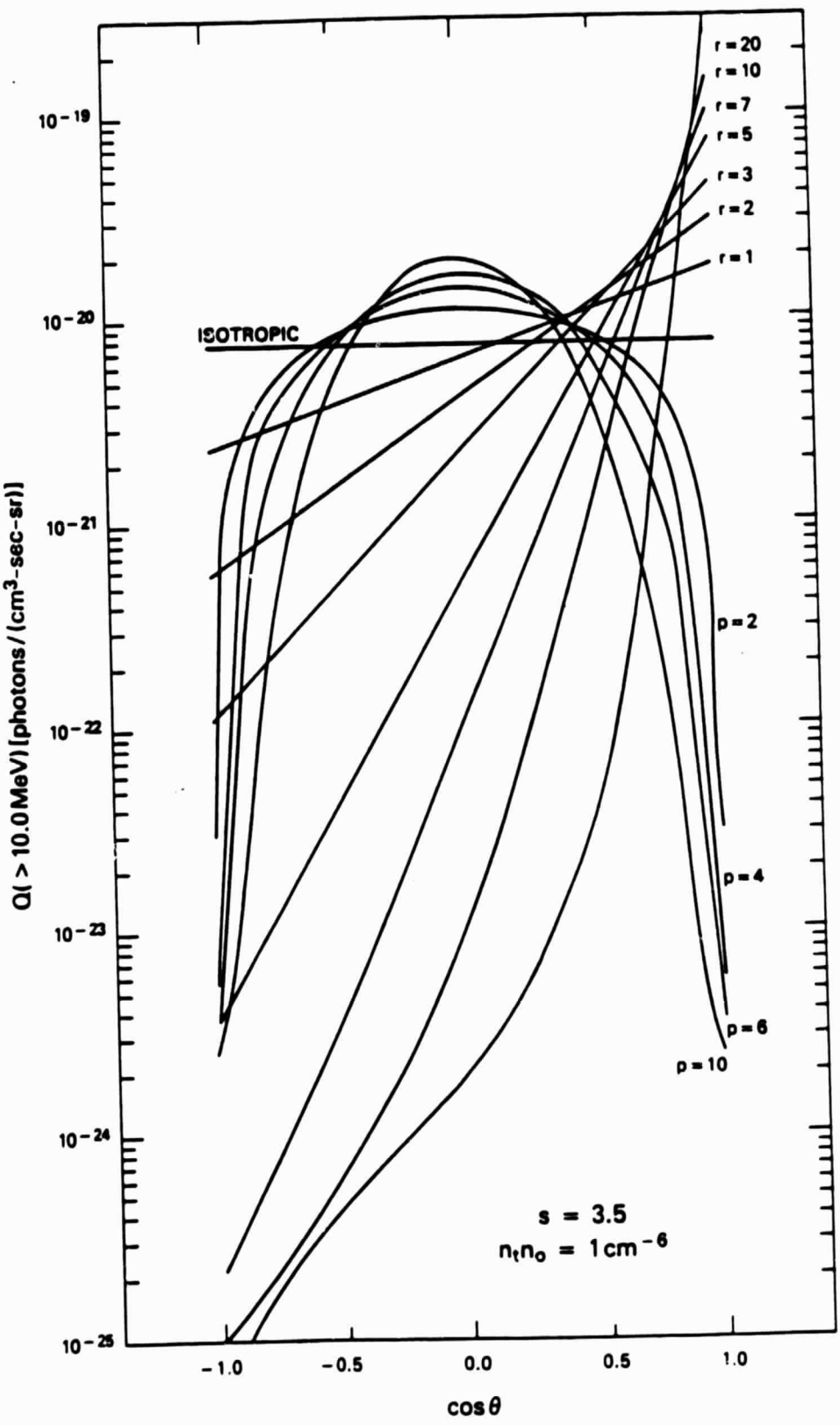
r = 20
r = 10
r = 7
r = 5
r = 3
r = 2
r = 1
ISOTROPIC
p = 2
p = 4
p = 6
p = 10
s = 3.5
$n_t n_o = 1 cm^{-6}$
10^{-19}
10^{-20}
10^{-21}
10^{-22}
10^{-23}
10^{-24}
10^{-25}
$Q(>10.0 MeV)$ [photons/$(cm^3$-sec-sr)]
-1.0
-0.5
0.0
0.5
1.0
$\cos\theta$

Fig. 15

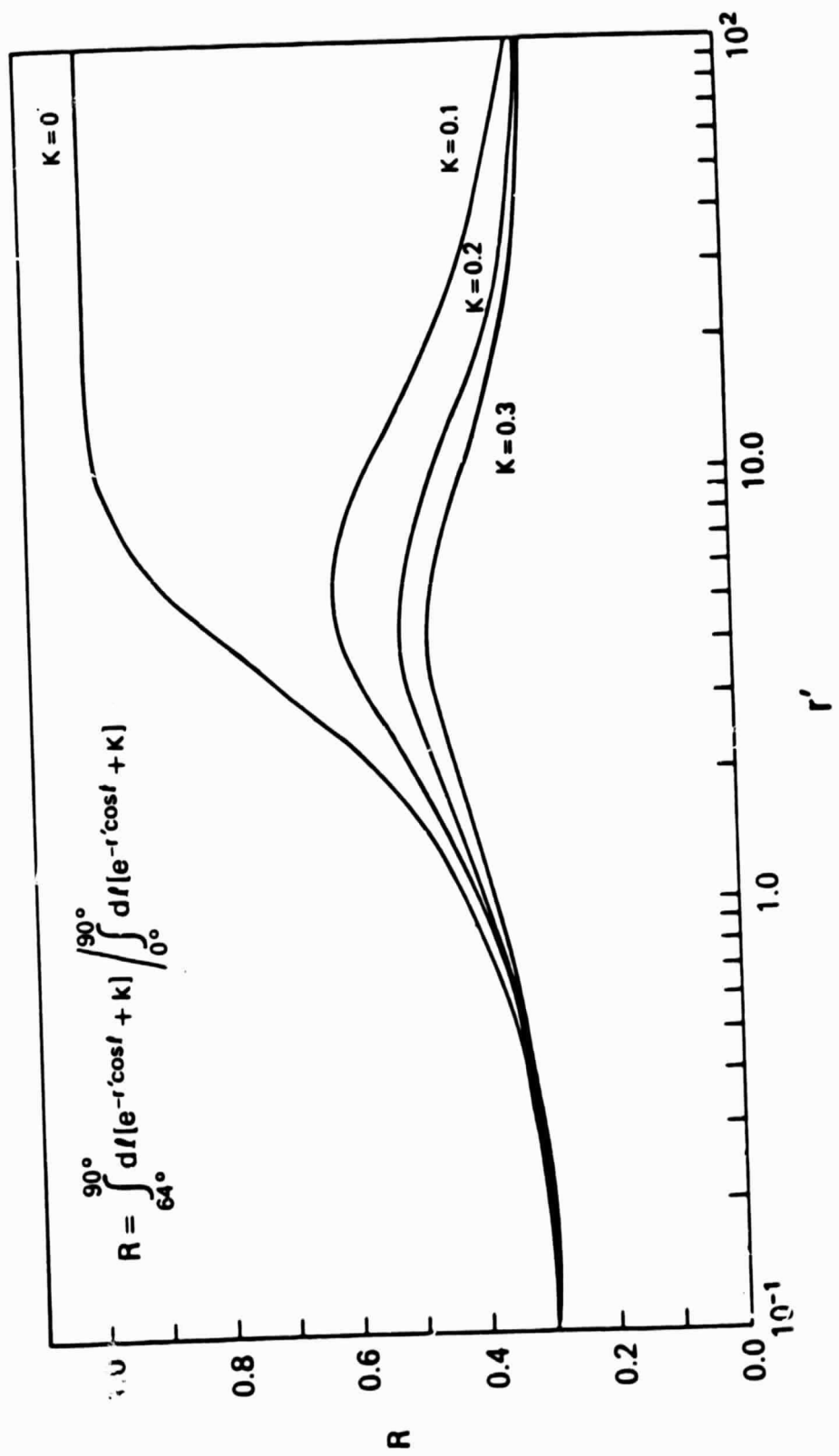
K=0
K=0.1
K=0.2
K=0.3
$R = \int_{64°}^{90°} df[e^{-r'\cos f} + K] \Big/ \int_{0°}^{90°} df[e^{-r'\cos f} + K]$
R
r'
0.0
0.2
0.4
0.6
0.8
1.0
10.0
10^{-1}
10^{2}

Fig. 16